arXiv:1301.6633v1 [nucl-ex] 28 Jan 2013

System Size Dependence of Transverse Momentum Correlations at RHIC

L. Adamczyk,[1] J. K. Adkins,[23] G. Agakishiev,[21] M. M. Aggarwal,[34] Z. Ahammed,[53] I. Alekseev,[19] J. Alford,[22] C. D. Anson,[31] A. Aparin,[21] D. Arkhipkin,[4] E. Aschenauer,[4] G. S. Averichev,[21] J. Balewski,[26] A. Banerjee,[53] Z. Barnovska,[14] D. R. Beavis,[4] R. Bellwied,[49] M. J. Betancourt,[26] R. R. Betts,[10] A. Bhasin,[20] A. K. Bhati,[34] Bhattarai,[48] H. Bichsel,[55] J. Bielcik,[13] J. Bielcikova,[14] L. C. Bland,[4] I. G. Bordyuzhin,[19] W. Borowski,[45] J. Bouchet,[22] A. V. Brandin,[29] S. G. Brovko,[6] E. Bruna,[57] S. Bültmann,[32] I. Bunzarov,[21] T. P. Burton,[4] J. Butterworth,[40] X. Z. Cai,[44] H. Caines,[57] M. Calderón de la Barca Sánchez,[6] D. Cebra,[6] R. Cendejas,[35] M. C. Cervantes,[47] P. Chaloupka,[13] Z. Chang,[47] S. Chattopadhyay,[53] H. F. Chen,[42] J. H. Chen,[44] J. Y. Chen,[9] L. Chen,[9] J. Cheng,[50] M. Cherney,[12] A. Chikanian,[57] W. Christie,[4] P. Chung,[14] J. Chwastowski,[11] M. J. M. Codrington,[48] R. Corliss,[26] J. G. Cramer,[55] H. J. Crawford,[5] X. Cui,[42] S. Das,[16] A. Davila Leyva,[48] L. C. De Silva,[49] R. R. Debbe,[4] T. G. Dedovich,[21] J. Deng,[43] R. Derradi de Souza,[8] S. Dhamija,[18] B. di Ruzza,[4] L. Didenko,[4] F. Ding,[6] A. Dion,[4] P. Djawotho,[47] X. Dong,[25] J. L. Drachenberg,[52] J. E. Draper,[6] C. M. Du,[24] L. E. Dunkelberger,[7] J. C. Dunlop,[4] L. G. Efimov,[21] M. Elnimr,[56] J. Engelage,[5] G. Eppley,[40] L. Eun,[25] O. Evdokimov,[10] R. Fatemi,[23] S. Fazio,[4] J. Fedorisin,[21] R. G. Fersch,[23] P. Filip,[21] E. Finch,[57] Y. Fisyak,[4] E. Flores,[6] C. A. Gagliardi,[47] D. R. Gangadharan,[31] D. Garand,[37] F. Geurts,[40] A. Gibson,[52] S. Gliske,[2] O. G. Grebenyuk,[25] D. Grosnick,[52] A. Gupta,[20] S. Gupta,[20] W. Guryn,[4] B. Haag,[6] O. Hajkova,[13] A. Hamed,[47] L-X. Han,[44] J. W. Harris,[57] J. P. Hays-Wehle,[26] S. Heppelmann,[35] A. Hirsch,[37] G. W. Hoffmann,[48] D. J. Hofman,[10] S. Horvat,[57] B. Huang,[4] H. Z. Huang,[7] P. Huck,[9] T. J. Humanic,[31] G. Igo,[7] W. W. Jacobs,[18] C. Jena,[30] E. G. Judd,[5] S. Kabana,[45] K. Kang,[50] J. Kapitan,[14] K. Kauder,[10] H. W. Ke,[9] D. Keane,[22] A. Kechechyan,[21] A. Kesich,[6] D. P. Kikola,[37] J. Kiryluk,[25] I. Kisel,[25] A. Kisiel,[54] S. R. Klein,[25] D. D. Koetke,[52] T. Kollegger,[15] J. Konzer,[37] I. Koralt,[32] W. Korsch,[23] L. Kotchenda,[29] P. Kravtsov,[29] K. Krueger,[2] I. Kulakov,[25] L. Kumar,[22] M. A. C. Lamont,[4] J. M. Landgraf,[4] K. D. Landry,[7] S. LaPointe,[56] J. Lauret,[4] A. Lebedev,[4] R. Lednicky,[21] J. H. Lee,[4] W. Leight,[26] M. J. LeVine,[4] C. Li,[42] W. Li,[44] X. Li,[37] X. Li,[46] Y. Li,[50] Z. M. Li,[9] L. M. Lima,[41] M. A. Lisa,[31] F. Liu,[9] T. Ljubicic,[4] W. J. Llope,[40] R. S. Longacre,[4] Y. Lu,[42] X. Luo,[9] A. Luszczak,[11] G. L. Ma,[44] Y. G. Ma,[44] D. M. M. D. Madagodagettige Don,[12] D. P. Mahapatra,[16] R. Majka,[57] S. Margetis,[22] C. Markert,[48] H. Masui,[25] H. S. Matis,[25] D. McDonald,[40] T. S. McShane,[12] S. Mioduszewski,[47] M. K. Mitrovski,[4] Y. Mohammed,[47] B. Mohanty,[30] M. M. Mondal,[47] M. G. Munhoz,[41] M. K. Mustafa,[37] M. Naglis,[25] B. K. Nandi,[17] Md. Nasim,[53] T. K. Nayak,[53] J. M. Nelson,[3] L. V. Nogach,[36] J. Novak,[28] G. Odyniec,[25] A. Ogawa,[4] K. Oh,[38] A. Ohlson,[57] V. Okorokov,[29] E. W. Oldag,[48] R. A. N. Oliveira,[41] D. Olson,[25] M. Pachr,[13] B. S. Page,[18] S. K. Pal,[53] Y. X. Pan,[7] Y. Pandit,[10] Y. Panebratsev,[21] T. Pawlak,[54] B. Pawlik,[33] H. Pei,[10] C. Perkins,[5] W. Peryt,[54] P. Pile,[4] M. Planinic,[58] J. Pluta,[54] N. Poljak,[58] J. Porter,[25] A. M. Poskanzer,[25] C. B. Powell,[25] C. Pruneau,[56] N. K. Pruthi,[34] M. Przybycien,[1] P. R. Pujahari,[17] J. Putschke,[56] H. Qiu,[25] S. Ramachandran,[23] R. Raniwala,[39] S. Raniwala,[39] R. L. Ray,[48] R. Redwine,[26] C. K. Riley,[57] H. G. Ritter,[25] J. B. Roberts,[40] O. V. Rogachevskiy,[21] J. L. Romero,[6] J. F. Ross,[12] L. Ruan,[4] J. Rusnak,[14] N. R. Sahoo,[53] P. K. Sahu,[16] I. Sakrejda,[25] S. Salur,[25] A. Sandacz,[54] J. Sandweiss,[57] E. Sangaline,[6] A. Sarkar,[17] J. Schambach,[48] R. P. Scharenberg,[37] A. M. Schmah,[25] B. Schmidke,[4] N. Schmitz,[27] T. R. Schuster,[15] J. Seele,[26] J. Seger,[12] P. Seyboth,[27] N. Shah,[7] E. Shahaliev,[21] M. Shao,[42] B. Sharma,[34] M. Sharma,[56] S. S. Shi,[9] Q. Y. Shou,[44] E. P. Sichtermann,[25] R. N. Singaraju,[53] M. J. Skoby,[18] D. Smirnov,[4] N. Smirnov,[57] D. Solanki,[39] P. Sorensen,[4] U. G. deSouza,[41] H. M. Spinka,[2] B. Srivastava,[37] T. D. S. Stanislaus,[52] S. G. Steadman,[26] J. R. Stevens,[26] R. Stock,[15] M. Strikhanov,[29] B. Stringfellow,[37] A. A. P. Suaide,[41] M. C. Suarez,[10] M. Sumbera,[14] X. M. Sun,[25] Y. Sun,[42] Z. Sun,[24] B. Surrow,[46] D. N. Svirida,[19] T. J. M. Symons,[25] A. Szanto de Toledo,[41] J. Takahashi,[8] A. H. Tang,[4] Z. Tang,[42] L. H. Tarini,[56] T. Tarnowsky,[28] J. H. Thomas,[25] J. Tian,[44] A. R. Timmins,[49] D. Tlusty,[14] M. Tokarev,[21] S. Trentalange,[7] R. E. Tribble,[47] P. Tribedy,[53] B. A. Trzeciak,[54] O. D. Tsai,[7] J. Turnau,[33] T. Ullrich,[4] D. G. Underwood,[2] G. Van Buren,[4] G. van Nieuwenhuizen,[26] J. A. Vanfossen, Jr.,[22] R. Varma,[17] G. M. S. Vasconcelos,[8] F. Videbæk,[4] Y. P. Viyogi,[53] S. Vokal,[21] S. A. Voloshin,[56] A. Vossen,[18] M. Wada,[48] F. Wang,[37] G. Wang,[7] H. Wang,[4] J. S. Wang,[24] Q. Wang,[37] X. L. Wang,[42] Y. Wang,[50] G. Webb,[23] J. C. Webb,[4] G. D. Westfall,[28] C. Whitten Jr.,[7] H. Wieman,[25] S. W. Wissink,[18] R. Witt,[51] Y. F. Wu,[9] Z. Xiao,[50] W. Xie,[37] K. Xin,[40] H. Xu,[24] N. Xu,[25] Q. H. Xu,[43] W. Xu,[7] Y. Xu,[42] Z. Xu,[4] L. Xue,[44] Y. Yang,[24] Y. Yang,[9] P. Yepes,[40] L. Yi,[37] K. Yip,[4] I-K. Yoo,[38] M. Zawisza,[54] H. Zbroszczyk,[54] J. B. Zhang,[9] S. Zhang,[44] X. P. Zhang,[50] Y. Zhang,[42] Z. P. Zhang,[42] F. Zhao,[7] J. Zhao,[44] C. Zhong,[44] X. Zhu,[50] Y. H. Zhu,[44] Y. Zoulkarneeva,[21] and M. Zyzak[25]

(STAR Collaboration)

[1] *AGH University of Science and Technology, Cracow, Poland*

[2]Argonne National Laboratory, Argonne, Illinois 60439, USA
[3]University of Birmingham, Birmingham, United Kingdom
[4]Brookhaven National Laboratory, Upton, New York 11973, USA
[5]University of California, Berkeley, California 94720, USA
[6]University of California, Davis, California 95616, USA
[7]University of California, Los Angeles, California 90095, USA
[8]Universidade Estadual de Campinas, Sao Paulo, Brazil
[9]Central China Normal University (HZNU), Wuhan 430079, China
[10]University of Illinois at Chicago, Chicago, Illinois 60607, USA
[11]Cracow University of Technology, Cracow, Poland
[12]Creighton University, Omaha, Nebraska 68178, USA
[13]Czech Technical University in Prague, FNSPE, Prague, 115 19, Czech Republic
[14]Nuclear Physics Institute AS CR, 250 68 Řež/Prague, Czech Republic
[15]University of Frankfurt, Frankfurt, Germany
[16]Institute of Physics, Bhubaneswar 751005, India
[17]Indian Institute of Technology, Mumbai, India
[18]Indiana University, Bloomington, Indiana 47408, USA
[19]Alikhanov Institute for Theoretical and Experimental Physics, Moscow, Russia
[20]University of Jammu, Jammu 180001, India
[21]Joint Institute for Nuclear Research, Dubna, 141 980, Russia
[22]Kent State University, Kent, Ohio 44242, USA
[23]University of Kentucky, Lexington, Kentucky, 40506-0055, USA
[24]Institute of Modern Physics, Lanzhou, China
[25]Lawrence Berkeley National Laboratory, Berkeley, California 94720, USA
[26]Massachusetts Institute of Technology, Cambridge, MA 02139-4307, USA
[27]Max-Planck-Institut für Physik, Munich, Germany
[28]Michigan State University, East Lansing, Michigan 48824, USA
[29]Moscow Engineering Physics Institute, Moscow Russia
[30]National Institute of Science Education and Research, Bhubaneswar 751005, India
[31]Ohio State University, Columbus, Ohio 43210, USA
[32]Old Dominion University, Norfolk, VA, 23529, USA
[33]Institute of Nuclear Physics PAN, Cracow, Poland
[34]Panjab University, Chandigarh 160014, India
[35]Pennsylvania State University, University Park, Pennsylvania 16802, USA
[36]Institute of High Energy Physics, Protvino, Russia
[37]Purdue University, West Lafayette, Indiana 47907, USA
[38]Pusan National University, Pusan, Republic of Korea
[39]University of Rajasthan, Jaipur 302004, India
[40]Rice University, Houston, Texas 77251, USA
[41]Universidade de Sao Paulo, Sao Paulo, Brazil
[42]University of Science & Technology of China, Hefei 230026, China
[43]Shandong University, Jinan, Shandong 250100, China
[44]Shanghai Institute of Applied Physics, Shanghai 201800, China
[45]SUBATECH, Nantes, France
[46]Temple University, Philadelphia, Pennsylvania, 19122
[47]Texas A&M University, College Station, Texas 77843, USA
[48]University of Texas, Austin, Texas 78712, USA
[49]University of Houston, Houston, TX, 77204, USA
[50]Tsinghua University, Beijing 100084, China
[51]United States Naval Academy, Annapolis, MD 21402, USA
[52]Valparaiso University, Valparaiso, Indiana 46383, USA
[53]Variable Energy Cyclotron Centre, Kolkata 700064, India
[54]Warsaw University of Technology, Warsaw, Poland
[55]University of Washington, Seattle, Washington 98195, USA
[56]Wayne State University, Detroit, Michigan 48201, USA
[57]Yale University, New Haven, Connecticut 06520, USA
[58]University of Zagreb, Zagreb, HR-10002, Croatia

We present a study of the average transverse momentum (p_t) fluctuations and p_t correlations for charged particles produced in Cu+Cu collisions at midrapidity for $\sqrt{s_{NN}} = 62.4$ and 200 GeV. These results are compared with those published for Au+Au collisions at same energies, to explore the system size dependence. In addition to the collision energy and system size dependence, the p_t correlations results have been studied as functions of the collision centralities, the ranges in p_t, the pseudo-rapidity η, and the azimuthal angle ϕ, for which the correlations are measured. The square root of the measured p_t correlations when scaled by mean-p_t are found to be independent of both colliding beam energy and system size studied. The transport based model calculations are found to have a better quantitative agreement with the measurements compared to models which incorporate only jet-like correlations.

PACS numbers: 25.75.Gz

I. INTRODUCTION

The study of event-by-event fluctuations and correlations is an important tool to understand thermalization and phase transitions in heavy-ion collisions [1–6]. Non-monotonic change in transverse momentum (p_t) correlations as a function of centrality and/or the incident energy has been proposed to be a possible signal of the Quark Gluon Plasma (QGP) formation [1]. The QGP is believed to be formed at the early stage of high energy heavy-ion collisions when the system is hot and dense. As the time passes, the system dilutes, cools down and hadronizes. Fluctuations are supposed to be sensitive to the dynamics of the system, especially at the QGP to hadron phase transition [4, 6]. Alternatively, analyses at the Relativistic Heavy Ion Collider (RHIC) based on p_t auto-correlations (the inversion of the mean transverse momentum fluctuations in different pseudorapidity and azimuthal angle difference regions of the produced particles) indicate that the basic correlation mechanism could be dominated by the process of parton fragmentation [7]. Thus fluctuation measurements are proposed to be an important tool in understanding the nucleus-nucleus collisions [1, 5, 6, 8–12]. In addition, under the assumption that thermodynamics is applicable to heavy-ion collisions, fluctuations in various observables could be related to thermodynamic properties of the matter formed. For example, the event-by-event $\langle p_t \rangle$ could be related to the temperature fluctuations [13–17].

The study of event-by-event fluctuations of various quantities such as event-wise mean transverse momentum ($\langle p_t \rangle$), charged track multiplicity, and conserved quantities such as net-baryon and/or net-charge are considered to be some of the main probes for the search of the critical point in the QCD phase diagram [17–26]. One expects enhanced fluctuations in the above observables when the system passes through the vicinity of the critical point. Recent results from the SPS experiments show that the energy dependence of transverse momentum fluctuations do not show the increase expected for freeze-out near the critical point of QCD [27]. However, when these fluctuations are studied as a function of the system size (colliding C+C, Si+Si, Pb+Pb), enhanced fluctuations are observed in smaller colliding systems [28]. The results from the RHIC Beam Energy Scan (BES) [29] data for the above observables will provide further insights.

The results presented here are from Cu+Cu collisions at $\sqrt{s_{NN}}$ = 62.4 and 200 GeV using the Solenoidal Tracker At RHIC (STAR) and are compared with the published results from Au+Au collisions at the same energies [30]. This paper describes a systematic study of the system size dependence of the transverse momentum correlations observed at RHIC.

The paper is organized as follows. In section II, we discuss the detectors, the data set, and the centrality selection used in the analysis. In section III, we discuss $\langle p_t \rangle$ fluctuations extracted from the $\langle p_t \rangle$ distributions, which are compared with mixed events and Gamma distributions. Dynamical fluctuations are extracted and presented for Au+Au and Cu+Cu collisions at $\sqrt{s_{NN}} = 62.4$ and 200 GeV. In section IV we discuss the p_t correlations, the dynamical correlations when scaled by $\langle N_{\rm part} \rangle$ and $\langle p_t \rangle$ to understand the centrality and energy dependence. We also compare the experimental data to various model calculations. Finally, we present a detailed study of η, ϕ and p_t dependence of the correlations. In section V, we discuss the systematic errors associated with the analysis presented. We conclude with a summary in section VI.

II. EXPERIMENT AND DATA ANALYSIS

The Cu+Cu data were taken using the STAR detector with a minimum bias trigger. For the data taken at $\sqrt{s_{NN}}$ = 200 GeV this was done by requiring a coincidence from the two Zero Degree Calorimeters (ZDCs). For the $\sqrt{s_{NN}}$ = 62.4 GeV data the ZDC is less efficient, so a Beam Beam Counter (BBC) coincidence was also required. More details about the trigger detectors can be obtained from Ref. [31].

The main detector used in this analysis is the Time Projection Chamber (TPC) [32], which is the primary tracking device in STAR. The TPC is 4.2 m long and 4 m in diameter and its acceptance spans about ±1.0 units of pseudorapidity and full azimuthal coverage. The sensitive volume of the TPC contains P10 gas (10% methane, 90% argon) regulated at 2 mbar above atmospheric pressure. The TPC data are used to determine particle trajectories, momenta, and particle-type through ionization energy loss (dE/dx) [33].

The primary vertex of events used in this analysis was required to be within ± 30 cm of the geometric center of the TPC along the beam axis. This selection process yielded about 7.5 M and 15 M minimum bias events for Cu+Cu collisions at $\sqrt{s_{NN}}$ = 62.4 and 200 GeV, respectively.

The collision centralities are represented by the fractions of events in the minimum bias inelastic cross section in a collision. In data, the collision centrality is determined by using the uncorrected charged track multiplicity ($N_{\rm ch}^{\rm TPC}$), measured in the TPC within $|\eta| < 0.5$.

The various centrality bins are calculated as a fraction of this multiplicity distribution starting at the highest multiplicities. The centrality classes for Cu+Cu collisions at $\sqrt{s_{NN}} = 62.4$ and 200 GeV are 0–10% (most central), 10–20%, 20–30%, 30–40% 40–50% and 50–60% (most peripheral). Each centrality bin is associated with an average number of participating nucleons ($\langle N_{\rm part}\rangle$) obtained using Glauber Monte Carlo simulations [34] employing the Woods-Saxon distribution for the nucleons inside the Cu nucleus. The systematic uncertainties are determined by varying the Woods-Saxon parameters and the uncertainties associated with nucleon-nucleon cross sections. Table I lists the $N_{\rm ch}^{\rm TPC}$ and $\langle N_{\rm part}\rangle$ values for each centrality in Cu+Cu collisions at $\sqrt{s_{NN}} = 62.4$ and 200 GeV. Corresponding values for Au+Au collisions can be found in Ref. [34].

TABLE I: The $N_{\rm ch}^{\rm TPC}$ values and average number of participating nucleons ($\langle N_{\rm part}\rangle$) for various collision centralities in Cu+Cu collisions at $\sqrt{s_{NN}} = 62.4$ and 200 GeV.

% cross	Cu+Cu 62.4 GeV		Cu+Cu 200 GeV	
section	$N_{\rm ch}^{\rm TPC}$	$\langle N_{\rm part}\rangle$	$N_{\rm ch}^{\rm TPC}$	$\langle N_{\rm part}\rangle$
0-10	> 101	$96.4^{+1.1}_{-2.6}$	> 139	$99.0^{+1.5}_{-1.2}$
10-20	$71 - 100$	$72.2^{+0.6}_{-1.9}$	$98 - 138$	$74.6^{+1.3}_{-1.0}$
20-30	$49 - 70$	$51.8^{+0.5}_{-1.2}$	$67 - 97$	$53.7^{+1.0}_{-0.7}$
30-40	$33 - 48$	$36.2^{+0.4}_{-0.8}$	$46 - 66$	$37.8^{+0.7}_{-0.5}$
40-50	$22 - 32$	$24.9^{+0.4}_{-0.6}$	$30 - 45$	$26.2^{+0.5}_{-0.4}$
50-60	$14 - 21$	$16.3^{+0.4}_{-0.3}$	$19 - 29$	$17.2^{+0.4}_{-0.2}$

In order to have uniform detector performance, a pseudorapidity cut of $|\eta| < 1.0$ is applied to tracks. To avoid the admixture of tracks from a secondary vertex, a requirement is placed on the distance of closest approach (DCA) between each track and the event vertex. The charged particle tracks are required to have originated within one cm of the measured event vertex. The multiple counting of split tracks (more than one track reconstructed from the original single track) is avoided by applying a condition on the number of track fit points ($N_{\rm Fit}$) used in the reconstruction of the track. We require that each included track had a minimum number of 21 TPC points along the track. The transverse momentum range selected for the analysis is 0.15–2.0 GeV/c.

The errors shown in the figures have the statistical and systematic errors added in quadrature unless otherwise stated. The statistical errors are small and are within symbol sizes. The final systematic errors are obtained as quadrature sums of systematic errors from different sources as discussed in section V.

III. $\langle p_t\rangle$ FLUCTUATIONS

The p_t fluctuations in high energy collisions can be measured using the distribution of the event-wise mean transverse momentum defined as

$$\langle p_t\rangle = \frac{1}{N}\sum_{i=1}^{N} p_{t,i}, \tag{1}$$

where N is the multiplicity of accepted tracks from the primary vertex in a given event and $p_{t,i}$ is the transverse momentum of the $i^{\rm th}$ track. The mean-p_t distribution is compared to the corresponding distribution obtained for "mixed events" [30]. Mixed events for a given centrality are constructed by randomly selecting one track from each event in that centrality while keeping the same event vertex. The total multiplicity for a given mixed event is kept the same as in the real data.

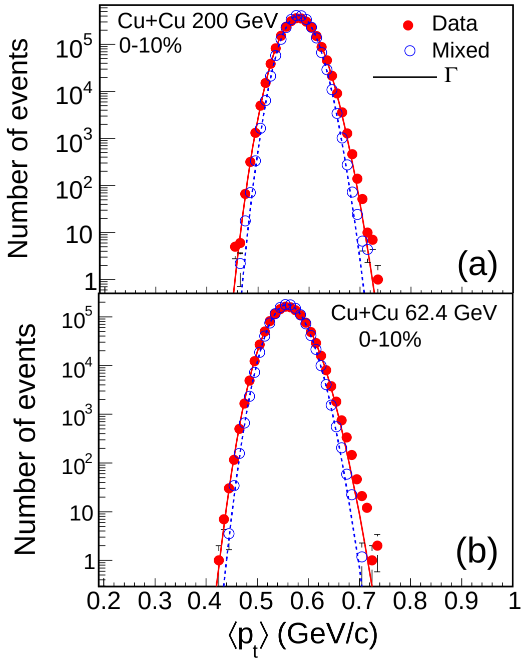

FIG. 1: (color online) Event-by-event $\langle p_t\rangle$ distributions for data and mixed events in central Cu+Cu collisions at (a) $\sqrt{s_{NN}} = 200$ and (b) 62.4 GeV. The curves (solid for data and dotted for mixed events) represent the Γ distributions. The errors shown are statistical.

Figure 1 shows the event-by-event mean-p_t distributions for 0-10% Cu+Cu collisions at (a) $\sqrt{s_{NN}} = 200$ and (b) 62.4 GeV. The solid symbols represent the $\langle p_t\rangle$ distributions for data; the open symbols represent $\langle p_t\rangle$ distributions for mixed events. The distributions are similar for other centralities. The mixed events provide reference to statistical fluctuations in the data. Any fluctuations observed in data beyond these statistical fluctuations are referred to as non-statistical or dynamical fluctuations in this paper. For both data and mixed events, as we go

TABLE II: Gamma distribution parameters for event-by-event mean-$\langle p_t \rangle$ distributions for data and mixed events in central (0-10%) Cu+Cu collisions at $\sqrt{s_{NN}}$ = 62.4 and 200 GeV.

Collision type (AA)	α	β ($\times 10^{-3}$ GeV/c)	μ (GeV/c)	σ (GeV/c)
Cu 200 (Data)	476	1.22	0.5805	0.02660
Cu 200 (Mixed)	634	0.92	0.5807	0.02310
Cu 62.4 (Data)	358	1.56	0.5603	0.02960
Cu 62.4 (Mixed)	457	1.23	0.5602	0.02621

from central to peripheral collisions, the mean (μ) of the distributions decreases while the width (σ), measured as the root mean square, increases. Moreover, it is seen that the $\langle p_t \rangle$ distributions for data are wider than those for mixed events, suggesting the presence of non-statistical fluctuations in Cu+Cu data for both 62.4 and 200 GeV collisions.

The curves in Fig. 1 represent the Gamma (Γ) distributions for data (solid lines) and mixed events (dotted lines). The Γ distribution [4, 35] is given by

$$f(x) = \frac{x^{\alpha-1} e^{-x/\beta}}{\Gamma(\alpha)\beta^{\alpha}}, \qquad (2)$$

where x represents the $\langle p_t \rangle$; $\alpha = \mu^2/\sigma^2$ and $\beta = \sigma^2/\mu$.

According to Ref. [35] the Γ distribution is one of the standard representations of the inclusive single particle p_t distribution. The author also suggests that the quantity $\alpha/\langle N_{\rm ch} \rangle$, should be ~ 2, and the quantity $\beta \times \langle N_{\rm ch} \rangle$ representing the inverse slope parameter may be referred to as the temperature of the system. Here $\langle N_{\rm ch} \rangle$ is the average charged particle multiplicity in a given centrality bin. We find that $\alpha/\langle N_{\rm ch} \rangle$ for Cu+Cu 0–10% central collisions at 200 GeV is 2.04 and that at 62.4 GeV is 2.18. The respective $\beta \times \langle N_{\rm ch} \rangle$ values are 0.284 GeV/c and 0.256 GeV/c. The $\alpha/\langle N_{\rm ch} \rangle$ and $\beta \times \langle N_{\rm ch} \rangle$ for 0–5% central Au+Au collisions at 200 GeV were found to be 1.93 and 0.299 GeV/c [30]. Table II lists Gamma distribution parameters for event-by-event $\langle p_t \rangle$ distributions for data and mixed events in central (0–10%) Cu+Cu collisions at $\sqrt{s_{NN}}$ = 62.4 and 200 GeV. The values for Au+Au collisions can be found in Ref. [30]. For Cu+Cu collisions at 200 GeV, $\alpha/\langle N_{\rm ch} \rangle$ varies from 2.04 to 2.11 from central to peripheral collisions. However, for Cu+Cu at 62.4 GeV, its values varies from 2.18 to 2.27 from central to peripheral collisions. The errors on values of α and β are of the order of 13–18% and 9-12%, respectively, for Cu+Cu collisions.

The non-statistical or dynamical fluctuations in mean-p_t are quantified using a variable $\sigma_{\rm dyn}$ [36, 37] defined as

$$\sigma_{\rm dyn} = \sqrt{\left(\frac{\sigma_{\rm data}}{\mu_{\rm data}}\right)^2 - \left(\frac{\sigma_{\rm mix}}{\mu_{\rm mix}}\right)^2}, \qquad (3)$$

where $\mu_{\rm data}$ and $\mu_{\rm mix}$ are the means of the event-by-event $\langle p_t \rangle$ distributions for data and mixed events, respectively. Similarly, $\sigma_{\rm data}$ and $\sigma_{\rm mix}$ are respectively the root mean square deviations in $\langle p_t \rangle$ distributions for data and mixed events. Figure 2 shows the dynamical fluctuations ($\sigma_{\rm dyn}$) in mean-p_t plotted as a function of $\langle N_{\rm part} \rangle$. The results are shown for Cu+Cu collisions at $\sqrt{s_{NN}}$ = 62.4 and 200 GeV, and are compared with the results from Au+Au collisions at $\sqrt{s_{NN}}$ = 62.4 and 200 GeV. The dynamical $\langle p_t \rangle$ fluctuations are similar in Au+Au and Cu+Cu collisions at similar values of $\langle N_{\rm part} \rangle$. The fluctuations decrease as the $\langle N_{\rm part} \rangle$ increases. The dynamical fluctuations are also independent of the collision energy and are found to vary from $\sim$ 2% to $\sim$ 5% for $\langle N_{\rm part} \rangle$ less than $\sim$120. For $\langle N_{\rm part} \rangle$ greater than $\sim$150, the dynamical fluctuations are smaller and vary from 1% to 2.5%.

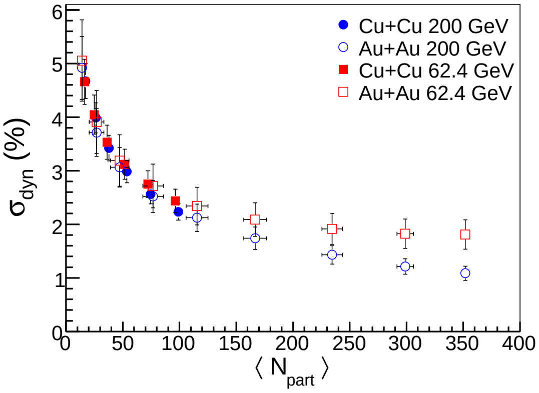

FIG. 2: (color online) Comparison of dynamical $\langle p_t \rangle$ fluctuations in Au+Au and Cu+Cu collisions at $\sqrt{s_{NN}}$ = 62.4 and 200 GeV as a function of number of participating nucleons.

IV. p_t CORRELATIONS

The non-statistical or dynamical fluctuations can also be analyzed by using the two-particle transverse momentum correlations [30]. The two-particle p_t correlations are studied using the following equation [30]:

$$\langle \Delta p_{t,i}\, \Delta p_{t,j} \rangle = \frac{1}{N_{\rm event}} \sum_{k=1}^{N_{\rm event}} \frac{C_k}{N_k(N_k-1)}, \qquad (4)$$

where C_k is the two-particle transverse momentum covariance for the $k^{\rm th}$ event,

$$C_k = \sum_{i=1}^{N_k} \sum_{j=1, i\neq j}^{N_k} (p_{t,i} - \langle\langle p_t \rangle\rangle)\,(p_{t,j} - \langle\langle p_t \rangle\rangle), \qquad (5)$$

$p_{t,i}$ is the transverse momentum of the $i^{\rm th}$ track in the $k^{\rm th}$ event, N_k is the number of tracks in the $k^{\rm th}$ event, and N_{event} is the number of events. The overall event average transverse momentum ($\langle\langle p_t\rangle\rangle$) is given by

$$\langle\langle p_t\rangle\rangle = \left(\sum_{k=1}^{N_{\mathrm{event}}} \langle p_t\rangle_k\right) / N_{\mathrm{event}}, \tag{6}$$

where $\langle p_t\rangle_k$ is the average transverse momentum in the k^{th} event. It may be noted that for mixed events, there will be no dynamical fluctuations and the p_t correlations will be zero. Equation (4) is used to obtain the p_t correlations in Cu+Cu collisions at $\sqrt{s_{NN}} = 62.4$ and 200 GeV. These results are compared with the published results from Au+Au collisions at similar energies [30] to investigate the system-size and collision energy dependence of the p_t correlations in heavy-ion collisions at RHIC.

The p_t correlation values may be affected by the dependence of the correlations on the size of the centrality bin and by changes induced due to a change in $\langle\langle p_t\rangle\rangle$. We removed this dependence by calculating $\langle\langle p_t\rangle\rangle$ as a function of $\langle N_{\mathrm{ch}}\rangle$. We fitted this dependence using a suitable polynomial function and used this fit in Eq. (5). All results presented in this paper have been corrected for this effect.

Figure 3 (a) shows the p_t correlations plotted as function of $\langle N_{\mathrm{part}}\rangle$ for Cu+Cu and Au+Au collisions at $\sqrt{s_{NN}} = 62.4$ and 200 GeV. We observe p_t correlations that decrease with increasing $\langle N_{\mathrm{part}}\rangle$ for Au+Au and Cu+Cu at both energies. The decrease in correlations with increasing participating nucleons could suggest that correlations are dominated by pairs of particles that originate from the same nucleon-nucleon collisions, and they get diluted when the number of participating nucleons increases [30].

A. Scaled p_t Correlations

The decrease in p_t correlations with increasing $\langle N_{\mathrm{part}}\rangle$ seen in Fig. 3 (a) may be related to a system volume dependence characterized by $\langle N_{\mathrm{part}}\rangle$. To remove this volume dependence we multiply the p_t correlations by $\langle N_{\mathrm{part}}\rangle/2$ as shown in Fig. 3 (b). The results are shown for Cu+Cu and Au+Au collisions at $\sqrt{s_{NN}} = 62.4$ and 200 GeV. It is observed that this measure of p_t correlations increases quickly with increasing collision centrality for both Cu+Cu and Au+Au collisions and saturates for central Au+Au collisions. The saturation of this quantity might indicate effects such as the onset of thermalization [26], the onset of jet quenching [3, 11], or the saturation of transverse flow in central collisions [38]. It seems that for Cu+Cu collisions this quantity is larger than for Au+Au collisions which might indicate more correlations for the smaller systems. But since the errors are large it is hard to make this conclusion.

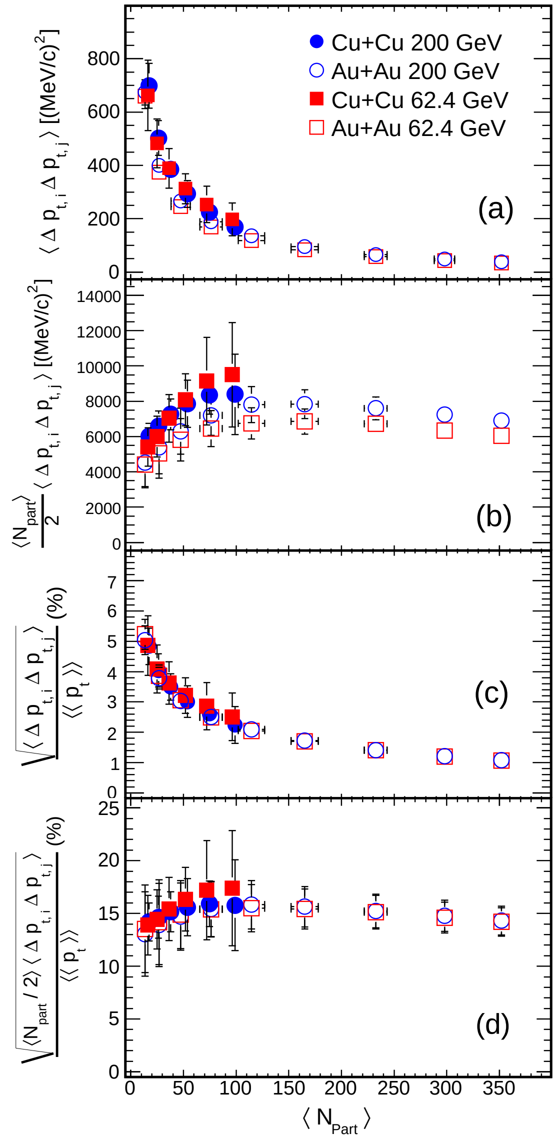

FIG. 3: (color online) (a) p_t correlations, (b) p_t correlations multiplied by $\langle N_{\mathrm{part}}\rangle/2$, (c) square root of p_t correlations scaled by $\langle\langle p_t\rangle\rangle$, and (d) square root of p_t correlations multiplied by $\langle N_{\mathrm{part}}\rangle/2$ and scaled by $\langle\langle p_t\rangle\rangle$, plotted vs. $\langle N_{\mathrm{part}}\rangle$. Results are compared between Cu+Cu and Au+Au collisions at $\sqrt{s_{NN}} = 62.4$ and 200 GeV. Au+Au data has been taken from the Ref. [30].

The correlation measure $\langle\Delta p_{t,i}\ \Delta p_{t,j}\rangle$ may change due to changes in $\langle\langle p_t\rangle\rangle$ with incident energy and/or collision centrality. To address these changes, we studied the square root of the measured correlations scaled by $\langle\langle p_t\rangle\rangle$. Figure 3 (c) shows the corresponding quantity $\sqrt{\langle\Delta p_{t,i}\ \Delta p_{t,j}\rangle}/\langle\langle p_t\rangle\rangle$ plotted as a function of collision centrality for Cu+Cu and Au+Au collisions at $\sqrt{s_{NN}} = 62.4$ and 200 GeV. It is observed that the correlation scaled by $\langle\langle p_t\rangle\rangle$ is independent of collision system size and energy, but decreases with increasing collision centrality. The combined effect of multiplying p_t correlations by $\langle N_{\mathrm{part}}\rangle/2$ and scaling with $\langle\langle p_t\rangle\rangle$ is shown in Fig. 3 (d). It seems that this quantity $\sqrt{\langle N_{\mathrm{part}}/2\rangle\langle\Delta p_{t,i}\ \Delta p_{t,j}\rangle}/\langle\langle p_t\rangle\rangle$

increases with $\langle N_{\rm part}\rangle$ and shows saturation for central Au+Au collisions, but is independent of collision system and energy.

B. Model Comparisons

It is interesting to compare the above results with theoretical model calculations to understand the physical mechanism behind these measurements. We compared our results with some widely used models in heavy-ion collisions such as Ultra Relativistic Quantum Molecular Dynamics model - UrQMD [39], A Multi Phase Transport model - AMPT (default and string-melting) [40], and Heavy-Ion Jet Interaction Generator - HIJING (with jet quenching switched off and on) [41]. We have used UrQMD ver.2.3, AMPT ver.1.11 for default, and ver.2.11 for AMPT string-melting.

HIJING is a perturbative QCD-inspired model that produces multiple minijet partons; these later get transformed into string configurations and then fragment to hadrons. The fragmentation is based on the Lund jet fragmentation model [42]. A parametrized parton-distribution function inside a nucleus is used to take into account parton shadowing.

The AMPT uses the same initial conditions as in HIJING. However, the minijet partons are made to undergo scattering before they are allowed to fragment into hadrons. The string-melting (SM) version of the AMPT model (labeled here as AMPT Melting) is based on the idea that for energy densities beyond a critical value of 1 GeV/fm^3, the system should be de-confined and strings (or hadrons) decomposed into their partonic components. This is done by converting the mesons to a quark-antiquark pair, baryons to three quarks, and so on. The scattering of the quarks is based on a parton cascade. Once the interactions stop, the partons then hadronize through the mechanism of parton coalescence. The UrQMD model is based on a microscopic transport theory where the phase-space description of the reactions is important. It allows for the propagation of all hadrons on classical trajectories in combination with stochastic binary scattering, color string formation, and resonance decay.

Figure 4 shows the comparison of p_t correlations between data ((a) and (c) for Au+Au 200 GeV, and (b) and (d) for Cu+Cu 200 GeV) and the models described above. We observe that the transport based UrQMD model calculations are found to have a better quantitative agreement with the measurements compared to models which incorporate only jet-like correlations as in HIJING. HIJING gives similar dependence on $\langle N_{\rm part}\rangle$ but under-predicts the magnitude. Inclusion of the jet-quenching effect in the HIJING leads to a smaller value of the correlations in central collisions. A multi-phase transport model calculation incorporating coalescence as a mechanism of particle production also compares well with data for central collisions. However the default

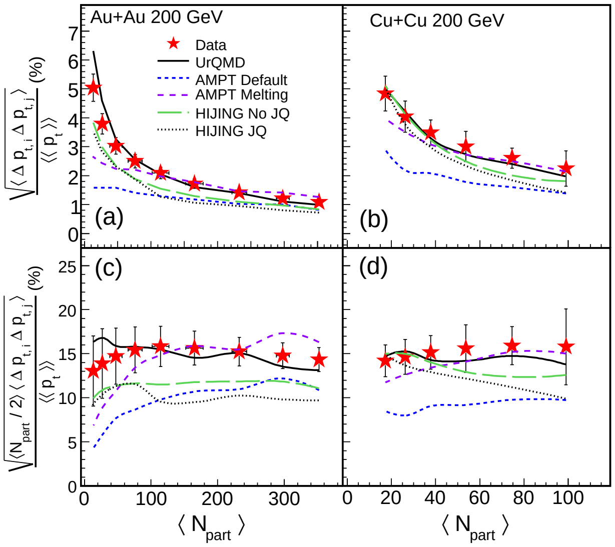

FIG. 4: (color online) Comparison of p_t correlations between data and models. Au+Au data has been taken from the Ref. [30]. The curves represent different model calculations.

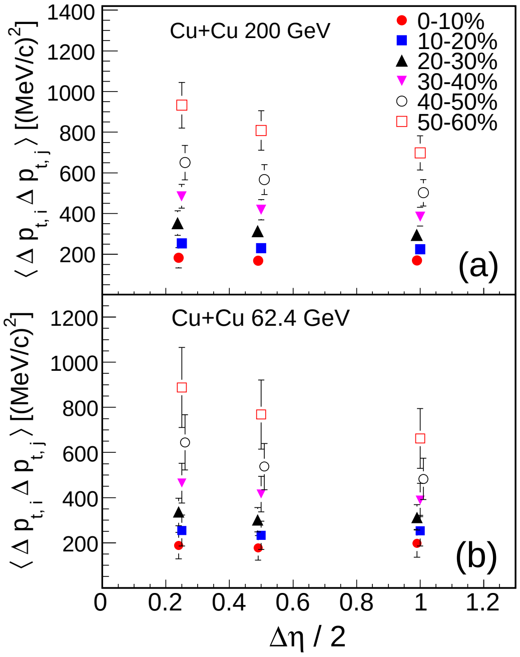

FIG. 5: (color online) p_t correlations for varying rapidity acceptance ($|\eta| < 0.25, 0.5, 1.0$) for Cu+Cu collisions at $\sqrt{s_{NN}} = 200$ and 62.4 GeV.

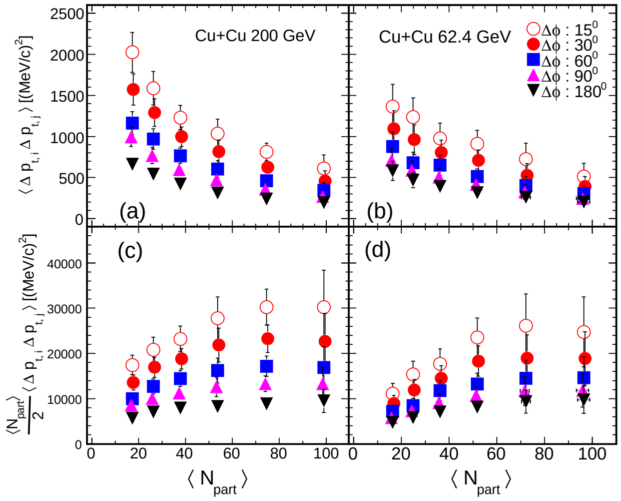

FIG. 6: (color online) p_t correlations for varying azimuthal acceptance for Cu+Cu collisions at $\sqrt{s_{NN}} = 200$ (panels (a) and (c)) and 62.4 GeV (panels (b) and (d)).

version of this model which incorporates additional initial and final state scattering relative to HIJING yields smaller values of correlations.

C. η and ϕ Dependence

The η and ϕ-dependences of p_t correlations were also studied. Figure 5 shows the p_t correlations plotted as a function of increasing rapidity acceptance for Cu+Cu collisions at (a) $\sqrt{s_{NN}} = 200$ and (b) 62.4 GeV. The data points for centralities 0-10%, 20-30%, and 40-50% are shifted by 0.01 in $\Delta\eta/2$ for clarity. The correlations are almost independent of the $\Delta\eta$ window for most central collisions. For peripheral collisions, the correlations show a slight rapidity dependence with maximum value for $-0.25 < \eta < 0.25$.

Figure 6 shows the p_t correlations for varying azimuthal angle windows for Cu+Cu collisions at (a) $\sqrt{s_{NN}} = 200$ and (b) 62.4 GeV. The data points for ϕ windows $\Delta\phi$: 30^0 and 90^0 are shifted by 0.5 units in $N_{\rm part}$ for clarity. We observe that the correlations are highest for the $\Delta\phi = 15^0$ (among the cases studied). The correlations decrease with increasing collision centrality for a given $\Delta\phi$ window as expected. The correlations multiplied by $\langle N_{\rm part}\rangle/2$ (Fig. 6 (c) for Cu+Cu 200 GeV and Fig. 6 (d) for Cu+Cu 62.4 GeV) seem to increase and then saturate with increasing collision centrality.

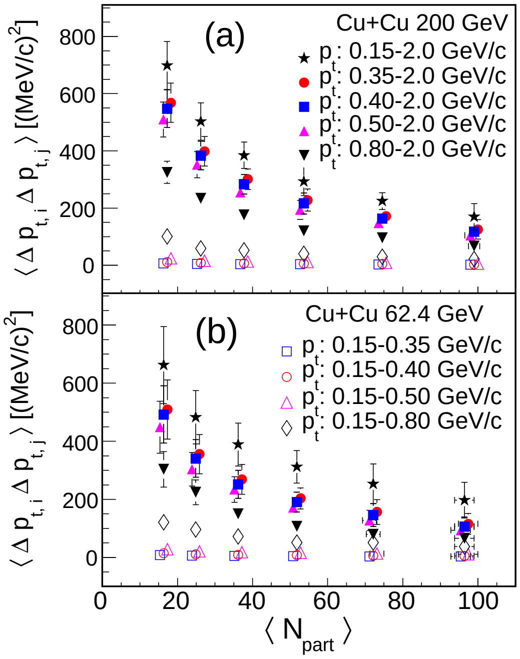

FIG. 7: (color online) p_t correlations for different p_t ranges shown for (a) Cu+Cu 200 GeV and (b) Cu+Cu 62.4 GeV.

D. p_t Dependence

Figure 7 shows the correlations as a function of collision centrality for different p_t regions for Cu+Cu collisions at (a) $\sqrt{s_{NN}} = 200$ and (b) 62.4 GeV. The different p_t ranges used are shown. The selection of these p_t ranges is done in order to see the dependence of p_t correlations among the lower p_t, higher p_t, and across higher and lower p_t tracks. The data points for p_t ranges (in GeV/c): 0.15-0.5, 0.5-2.0, 0.15-0.35, and 0.35-2.0, are shifted by one unit in $\langle N_{\rm part}\rangle$.

We observe that p_t correlation is maximum (minimum) for charged particles whose p_t is between 0.15–2.0 GeV/c (0.15–0.35 GeV/c). The p_t correlation values are small and fairly independent of p_t if a lower p_t bound for the particles studied is fixed at 0.15 GeV/c and the upper p_t bound is progressively increased up to 0.50 GeV/c. When the analysis is carried out by keeping the higher p_t bound fixed at 2.0 GeV/c and subsequently decreasing the lower p_t bound to 0.15 GeV/c, the correlation values are found to increase.

Figure 8 shows the variation of p_t correlations as a function of $\langle N_{\rm part}\rangle$ for different p_t windows as calculated using the (a) AMPT (string-melting), (b) UrQMD, and (c) HIJING (no jet quenching) model calculations for Cu+Cu collisions at 200 GeV. The AMPT calculations show p_t correlations that are similar to those ob-

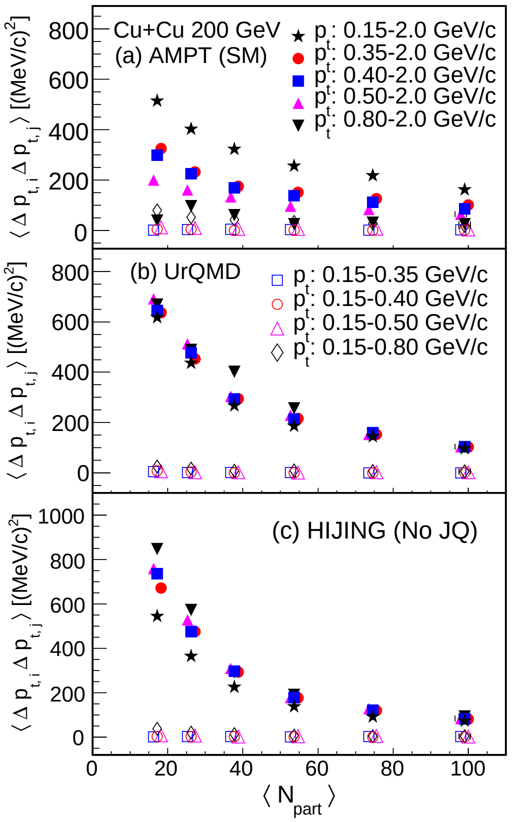

FIG. 8: (color online) Correlations for varying p_t ranges for different model calculations in Cu+Cu 200 GeV: (a) AMPT (SM), (b) UrQMD, and (c) Hijing (No JQ).

served in data for corresponding variations in the p_t windows. The trend of the correlation values shown by both UrQMD and HIJING is similar to what is seen in the data for the low-p_t windows where the lower bound is fixed at 0.15 GeV/c and the upper bound is increased from 0.35 GeV/c to 0.50 GeV/c. However, for UrQMD, if the higher p_t bound is fixed at 2.0 GeV/c and the lower p_t bound is subsequently decreased to 0.15 GeV/c, p_t correlation values remain similar. For the same case, HIJING shows decrease in p_t correlation values when the lower p_t bound is decreased to 0.15 GeV/c. This is just opposite of what was observed in data as seen in Fig. 7.

Because we calculate correlations for different p_t ranges, we have examined the p_t acceptance effects on the observed p_t correlations. The correlation values in different p_t ranges may depend on the p_t range size and on the fluctuations in the p_t spectrum slope in that p_t range. It is, therefore, important to see the effect of slope fluctuations on the correlation values in different p_t ranges. The p_t correlations can be formulated in terms of the fluctuations in the inverse slope parameter (effective

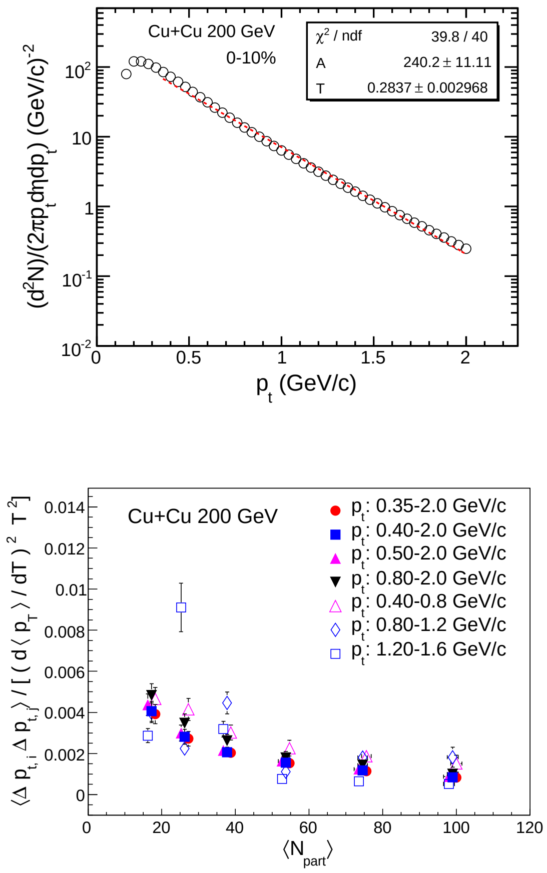

FIG. 9: (color online) Top panel: Uncorrected inclusive charged particle p_t spectrum for 0-10% collision centrality for Cu+Cu 200 GeV (open circles). The distribution is fit to the exponential function: $Ae^{-p_t/T}$ (red dashed-line). Errors are statistical. Bottom panel: Correlations scaled by $(d\langle p_t\rangle/dT)^2T^2$ vs. $\langle N_{\text{part}}\rangle$ for different p_t ranges in Cu+Cu 200 GeV.

temperature) by the following relation [17]:

$$\langle \Delta p_t \; \Delta p_t \rangle \approx \left[\frac{d\langle p_t\rangle}{dT}\right]^2 \Delta T^2, \qquad (7)$$

where ΔT^2 describes the fluctuation in the inverse slope parameter. The dependence $\langle p_t(T)\rangle$ can be obtained from the function that describes the inclusive uncorrected p_t spectrum for the desired p_t range in the following manner. Figure 9 (top panel) shows the measured inclusive p_t spectrum for 0–10% collision centrality in Cu+Cu collisions at 200 GeV. The dotted curve represents the exponential fit of the form $F(p_t) = Ae^{-p_t/T}$, that is fit to these measurements for the p_t range 0.35–2.0 GeV/c. The expression for $\langle p_t\rangle$ and $(d\langle p_t\rangle/dT)$ can be obtained using the following relation:

$$\langle p_t \rangle = \frac{\displaystyle\int_a^b p_t^2 F(p_t) dp_t}{\displaystyle\int_a^b p_t F(p_t) dp_t}, \tag{8}$$

which gives,

$$\langle p_t \rangle = 2T + \frac{a^2 e^{-a/T} - b^2 e^{-b/T}}{(a+T)e^{-a/T} - (b+T)e^{-b/T}}. \tag{9}$$

Here, a and b are respectively the lower and upper limits of a given p_t range. The derivative of $\langle p_t \rangle$ with respect to T is obtained as:

$$\frac{d\langle p_t \rangle}{dT} = 2 - \frac{Ae^{-(a+b)/T} + a^2 e^{-2a/T} + b^2 e^{-2b/T}}{[(a+T)e^{-a/T} - (b+T)e^{-b/T}]^2}, \tag{10}$$

where

$$A = \frac{ab(b-a)^2}{T^2} + \frac{(b^2-a^2)(b-a)}{T} - (a^2+b^2). \tag{11}$$

Using the lower and upper limits of a given p_t range, the corresponding T from the spectrum fit for each p_t range and collision centrality, we can obtain $(d\langle p_t \rangle/dT)^2$ for every p_t range in each centrality.

Figure 9 (bottom panel) shows the measured two-particle p_t correlations scaled by $(d\langle p_t \rangle/dT)^2 T^2$ vs. $\langle N_{\rm part} \rangle$ for different p_t ranges in Cu+Cu 200 GeV. The data points for p_t ranges (in GeV/c): 0.4-0.8, 0.5-2.0, 1.2-1.6, and 0.35-2.0, are shifted by one unit in $\langle N_{\rm part} \rangle$ for clarity. We observe that scaled p_t correlations for different p_t ranges become similar and show little dependence on the collision centrality. This study seems to suggest that the difference in the p_t correlations for different p_t ranges is due to the fluctuations in slope of the p_t spectrum in those p_t ranges.

V. SYSTEMATIC UNCERTAINTIES

Systematic errors on the mean (μ) and root mean square deviations (σ) in the $\langle p_t \rangle$ distributions (discussed in section III), and p_t correlations (discussed in section IV) are mainly evaluated by varying the different cuts used in the analysis, re-doing analysis using these changed cuts and determining the resulting changes in the values of μ, σ, and the p_t correlations. The difference is taken as the systematic error due to a particular analysis cut. The resulting systematic uncertainties, described below, are shown in Tables III and IV as a percentage of the result (μ, σ, and the p_t correlations) for various centralities for Cu+Cu collisions at both 62.4 and 200 GeV.

To study the effect of the z-vertex (V_z) cut we increased the V_z acceptance to ± 50 cm from the default value of ±30 cm. We observed no change in μ or σ or in the p_t correlations when using the wider V_z.

TABLE III: Systematic errors on μ and σ in event-wise $\langle p_t \rangle$ distributions as described in section V for various collision centralities in Cu+Cu collisions at $\sqrt{s_{NN}}$ = 62.4 and 200 GeV.

	Cu+Cu 62.4 GeV				Cu+Cu 200 GeV			
% cross section	DCA μ (%)	$N_{\rm Fit}$ μ (%)	DCA σ (%)	$N_{\rm Fit}$ σ (%)	DCA μ (%)	$N_{\rm Fit}$ μ (%)	DCA σ (%)	$N_{\rm Fit}$ σ (%)
0-10	3.6	0.4	7.9	1.0	3.4	0.24	5.7	1.2
10-20	3.6	0.4	7.1	1.0	3.3	0.23	5.2	1.2
20-30	3.6	0.4	6.6	1.0	3.3	0.23	5.2	1.1
30-40	3.6	0.4	6.2	1.0	3.3	0.20	4.7	1.2
40-50	3.6	0.4	6.0	1.0	3.2	0.20	4.9	1.1
50-60	3.6	0.4	6.0	1.0	3.2	0.22	4.4	1.2

TABLE IV: Systematic errors on p_t correlations as described in section V for various collision centralities in Cu+Cu collisions at $\sqrt{s_{NN}}$ = 62.4 GeV and 200 GeV.

	Cu+Cu 62.4 GeV				Cu+Cu 200 GeV			
% cross section	DCA (%)	$N_{\rm Fit}$ (%)	Poly. (%)	Low p_t (%)	DCA (%)	$N_{\rm Fit}$ (%)	Poly. (%)	Low p_t (%)
0-10	30	1.4	1.9	7.2	16	0.05	1.9	22
10-20	23	0.8	3.6	13.1	13	0.09	3.6	3.2
20-30	18	0.6	1.9	3.4	13	1.1	1.9	12.3
30-40	17	1.0	0.004	9.0	8	1.2	0.004	9.7
40-50	19	3.0	0.009	1.0	10	2.0	0.009	8.4
50-60	20	3.6	0.009	4.0	7	5.0	0.009	8.3

The effect of the cuts used to suppress background tracks was studied by changing the DCA cut from the default, DCA < 1 cm, to DCA < 1.5 cm and separately, changing the required number of fit points along the track, $N_{\rm Fit}$, from the default $N_{\rm Fit} > 20$ to $N_{\rm Fit} > 15$. The resulting systematic errors due to these changes are listed in Tables III and IV in the columns labeled "DCA" and "$N_{\rm Fit}$".

The effect of the size of the centrality bin on the p_t correlations was addressed by fitting $\langle\langle p_t \rangle\rangle$ as a function of $\langle N_{\rm ch} \rangle$ (see section IV). To determine the systematic uncertainty associated with this process we used different polynomial functions to fit $\langle\langle p_t \rangle\rangle$ vs. $\langle N_{\rm ch} \rangle$. The systematic errors associated with this correction are listed in Table IV in the columns labeled "Poly.".

We estimated the systematic uncertainty on the p_t correlations that may be associated with the application of the low-p_t cut by removing this p_t cut in the HIJING[41] model calculations. The estimated systematic errors are shown in Table IV in the columns labeled "Low p_t".

The p_t correlations may also include the short range correlations such as Coulomb interactions and Hanbury Brown-Twiss (HBT) correlations. These correlations usually dominate between the pairs of particles having relative transverse momentum less than 100 MeV/c. The effect of these short-range correlations on the measured p_t correlations is seen by calculating p_t correlations after removing the pairs of particles with relative momentum $(p_i - p_j)$, less than 100 MeV/c. We observed that the p_t correlations are reduced by maximum of 6% when short-range correlations are excluded.

The p_t correlations also include the contributions from resonance decays and charge ordering. These correlations are obtained for pairs of particles having like ($++$ or $--$) and unlike ($+-$) charges with respect to inclusive charged particles. A maximum of 15% decrease in the correlations is observed for pairs of particles with like charges and about 12% increase is observed for pairs with unlike charges with respect to the correlations for inclusive charged particle pairs for Cu+Cu collisions at $\sqrt{s_{NN}} = 62.4$ GeV and 200 GeV.

VI. SUMMARY

We have reported the measurements of p_t fluctuations in Cu+Cu collisions in the STAR detector at RHIC for $\sqrt{s_{NN}} = 62.4$ and 200 GeV, and compared with Au+Au collisions at the same energies to investigate the system size dependence. We have observed dynamical p_t fluctuations by comparing data to mixed events in both Cu+Cu and Au+Au collisions at these two beam energies. Moreover, for similar mean number of participating nucleons, the p_t fluctuations are observed to be comparable for the Cu+Cu and Au+Au systems, suggesting that the system size has little effect. In addition, we have compared p_t correlation measurements for Cu+Cu collisions at $\sqrt{s_{NN}} = 62.4$ and 200 GeV with the published Au+Au measurements. We found that for both Cu+Cu and Au+Au systems the p_t correlation decreases with increasing $\langle N_{\text{part}} \rangle$ at both beam energies. The dilution of the p_t correlations with increasing $\langle N_{\text{part}} \rangle$ could be due to the decrease in correlations that are dominated by pairs of particles that originate from the same nucleon-nucleon collision. A similar observation is found with other fluctuation and correlation observables like K/π [37] and net-charge [43].

The p_t correlations were found to scale with number of participating nucleon pairs for $\langle N_{\text{part}} \rangle > 100$ (when the system size is larger than that of central Cu+Cu collisions). This might indicate the onset of thermalization [26], the onset of jet quenching [3, 11], or the saturation of transverse flow in central collisions [38]. The square root of the p_t correlations normalized by event-wise average transverse momentum for Cu+Cu and Au+Au collisions is similar for systems with similar $\langle N_{\text{part}} \rangle$ and is independent of the beam energies studied.

The results described above are compared to predictions from several relevant model calculations. The transport based UrQMD model calculations are found to have a better quantitative agreement with the measurements compared to models which incorporate only jet-like correlations as in HIJING. HIJING gives similar dependence on $\langle N_{\text{part}} \rangle$, but under-predicts the magnitude. Inclusion of the jet-quenching effect in the HIJING leads to a smaller value of the correlations in central collisions. A multi-phase transport model calculation incorporating coalescence as a mechanism of particle production also compares well with data for central collisions.

When studying the p_t correlations for different p_t intervals, the correlations appear to be small and fairly independent of p_t interval, if we fix the lower p_t bound at 0.15 GeV/c and progressively increase the higher p_t bound up to 0.50 GeV/c. This suggests that correlations are weak for low-p_t particles. This low-p_t trend observed in the data is also seen in UrQMD, AMPT, and HIJING models. When the analysis is carried out keeping the higher p_t bound fixed at 2.0 GeV/c and progressively decreasing the lower p_t bound to $p_t = 0.15$ GeV/c, the correlation values in data are found to increase. This suggests that high p_t particles are more correlated with low-p_t particles. The AMPT model shows a rather similar variation of p_t correlations for different p_t intervals, as observed in data. The UrQMD model calculations, however, show no such variations in correlations for the different p_t intervals with higher p_t bound fixed at 2.0 GeV/c. Finally, we note that the HIJING model calculations give p_t correlations that decrease with a decrease in the lower p_t bound for intervals with fixed higher p_t (= 2.0 GeV/c) bound that is opposite to what is observed in data. We tried to understand the changes in p_t correlations in different p_t intervals as observed in data. We observed that the resultant fluctuations after considering event-by-event variation in the slope of the p_t spectra for different p_t bins were all of similar order.

We have also shown the variation of the p_t correlation with the change in the accepted range of pseudorapidity and azimuthal angle of the produced particles. We observed that the correlation values increase when the η- and ϕ-acceptance are reduced.

We thank the RHIC Operations Group and RCF at BNL, the NERSC Center at LBNL and the Open Science Grid consortium for providing resources and support. This work was supported in part by the Offices of NP and HEP within the U.S. DOE Office of Science, the U.S. NSF, the Sloan Foundation, CNRS/IN2P3, FAPESP CNPq of Brazil, Ministry of Ed. and Sci. of the Russian Federation, NNSFC, CAS, MoST, and MoE of China, GA and MSMT of the Czech Republic, FOM and NWO of the Netherlands, DAE, DST, and CSIR of India, Polish Ministry of Sci. and Higher Ed., National Research Foundation (NRF-2012004024), Ministry of Sci., Ed. and Sports of the Rep. of Croatia, and RosAtom of Russia.

---

[1] H. Heiselberg, Phys. Rep. **351**, 161 (2001).
[2] H. Appelshauser *et al.* (NA49 Collaboration), Phys. Lett. B **459**, 679 (1999); D. Adamova *et al.* (CERES Collaboration), Nucl. Phys. A **727**, 97 (2003); J. Adams *et al.* (STAR Collaboration), Phys. Rev. C **71**, 064906 (2005); K. Adcox *et al.* (PHENIX Collaboration), Phys. Rev. Lett. **89**, 212301 (2002).
[3] S. S. Adler et al. (PHENIX Collaboration), Phys. Rev. Lett. **93**, 092301 (2004).
[4] J. Adams *et al.* (STAR Collaboration), Phys. Rev. C **71**, 064906 (2005).
[5] M. M. Aggarwal *et al.* (WA98 Collaboration), Phys. Rev. C **65**, 054912 (2002).
[6] K. Adcox *et al.* (PHENIX Collaboration), Phys. Rev. C **66**, 024901 (2002).
[7] J. Adams *et al.*,(STAR Collaboration), J. Phys. G **34**, 451 (2007); J. Phys. G **32**, L37 (2006).
[8] M. Stephanov, K. Rajagopal and E. Shuryak, Phys. Rev. Lett. **81**, 4816 (1998).
[9] M. Stephanov, K. Rajagopal and E. Shuryak, Phys. Rev. D **60**, 114028 (1999).
[10] M. Stephanov, Phys. Rev. D **65**, 096008 (2002).
[11] Q. Liu and T. A. Trainor, Phys. Lett. B **567**, 184 (2003).
[12] J. D. Bjorken and E. A. Paschos, Phys. Rev. **185**, 1975 (1969).
[13] L. Stodolsky, Phys. Rev. Lett. **75**, 1044 (1995).
[14] S. Mrowczynski, Phys. Lett. B **430**, 9 (1998).
[15] K. Rajagopal, proc. of the Minnesota conference on Continuous Advances in QCD 1998 (hep-ph/9808348).
[16] B. Berdnikov and K. Rajagopal, Phys. Rev. D. **61**, 105017 (2000);
[17] S. A. Voloshin, V. Koch and H. G. Ritter, Phys. Rev. C **60**, 024901 (1999).
[18] S. A. Bass, M. Gyulassy, H. Stöcker and W. Greiner, J. Phys. G **25**, R1 (1999).
[19] S. A. Bass, P. Danielewicz and S. Pratt, Phys. Rev. Lett. **85**, 2689 (2000).
[20] S. Jeon and V. Koch, Phys. Rev. Lett. **85**, 2076 (2000).
[21] M. Asakawa, U. Heinz and B. Müller, Phys. Rev. Lett. **85**, 2072 (2000).
[22] Z.-W. Lin and C. M. Ko, Phys. Rev. C **64**, 041901(R) (2001).
[23] H. Heiselberg and A. D. Jackson, Phys. Rev. C **63**, 064904 (2001).
[24] E. V. Shuryak and M. A. Stephanov, Phys. Rev. C **63**, 064903 (2001).
[25] C. Pruneau, S. Gavin and S. Voloshin, Phys. Rev. C **66**, 044904 (2002).
[26] S. Gavin, Phys. Rev. Lett. **92**, 162301 (2004).
[27] M. Rybczynski *et al.* (for NA49 Collaboration), J. Phys. G **35**, 104091 (2008).
[28] T. Anticic *et al.* (NA49 Collaboration), Phys. Rev. C 79, 044904 (2009); K. Grebieszkow (for the NA49 and NA61 Collaborations), Acta Phys. Polon. B 41, 427 (2010).
[29] B. I. Abelev *et al.* (STAR Collaboration), Phys. Rev. C **81**, 024911 (2010); STAR Internal Note-SN0493, 2009; arXiv:1007.2613; L. Kumar (STAR Collaboration), Nucl. Phys. A **830**, 275C (2009); ibid **862**, 125 (2011); B. Mohanty, Nucl. Phys. A **830**, 899C (2009).
[30] J. Adams *et al.* (STAR Collaboration), Phys. Rev. C **72**, 044902 (2005).
[31] F. S. Bieser *et al.*, Nucl. Instr. Meth. A **499**, 766 (2003).
[32] K. H. Ackermann *et al.* (STAR Collaboration), Nucl. Instr. Meth. A **499**, 624 (2003).
[33] H. Bichsel, Nucl. Instr. Meth. A **562**, 154 (2006).
[34] B. I. Abelev *et al.* (STAR Collaboration), Phys. Rev. C **79**, 034909 (2009); D. Kharzeev and M. Nardi, Phys. Lett. B **507**, 121 (2001).
[35] M. J. Tannenbaum, Phys. Lett. B **498**, 29 (2001).
[36] S. V. Afanasiev *et al.* (NA49 Collaboration), Phys. Rev. Lett. **86**, 1965 (2001).
[37] B. I. Abelev *et al.* (STAR Collaboration), Phys. Rev. Lett. **103**, 092301 (2009).
[38] S. A. Voloshin, Phys. Lett. B **632**, 490 (2006).
[39] S. A. Bass *et al.*, Prog. Part. Nucl. Phys. **41**, 255 (1998); M. Bleicher *et al.*, J. Phys. G **25**, 1859 (1999).
[40] Z.-W. Lin and C. M. Ko, Phys. Rev. C **65**, 034904 (2002); Z.-W. Lin, C. M. Ko, B. A. Li, B. Zhang, and S. Pal, *ibid.* **72**, 064901 (2005); L.-W. Chen *et al.*, Phys. Lett. B **605**, 95 (2005).
[41] X. N. Wang and M. Gyulassy, Phys. Rev. D **44**, 3501 (1991).
[42] B. Andersson, G. Gustafson, G. Ingelman, and T. Sjostrand, Phys. Rep. **97**, 31 (1983).
[43] B. I. Abelev *et al.* (STAR Collaboration), Phys. Rev. C **79**, 024906 (2009).